Research Square

Preprints are preliminary reports that have not undergone peer review.
They should not be considered conclusive, used to inform clinical practice,
or referenced by the media as validated information.

An Alternative Electrochemical Approach to Detect 4-Nitrophenylhydrazine With ZnO/SnO2 Nanoparticles Decorated Glassy Carbon Electrode

Md Mahmud Alam (alam-mahmud@hotmail.com)
Shahjalal University of Science and Technology https://orcid.org/0000-0002-2636-5038
M.T. Uddin
Shahjalal University of Science and Technology
Mohammed M. Rahman
King Abdulaziz University
Abdullah M. Asiri
King Abdulaziz University
M.A. Islam
Shahjalal University of Science and Technology

Research Article

Keywords: ZnO/SnO2 nanoparticles, Glassy carbon electrode, 4-Nitrophenylhydrazine sensor, Sensitivity, Environmental protection

Posted Date: February 15th, 2021

DOI: https://doi.org/10.21203/rs.3.rs-193392/v1

License: This work is licensed under a Creative Commons Attribution 4.0 International License.
Read Full License

Abstract

The 4-NPHyd (4-nitrophenylhydrazine) electrochemical sensor assembled using wet-chemically prepared ZnO/SnO_2 nanoparticle (NPs) decorated a glassy carbon electrode (GCE) with conductive Nafion binder. The synthesized NPs characterized by XPS, ESEM, EDS, and XRD analysis. The calibration of the proposed sensor obtained from current versus concentration of 4-NPHyd found linear over a concentration (0.1nM~0.01mM) of 4-NPHyd, which denoted as the dynamic range (LDR) for detection of 4-NPHyd. The 4-NPHyd sensor sensitivity calculated using the LDR slope considering the active surface of GCE (0.0316 cm2), which is equal to be 7.6930 μAμM-1cm-2, an appreciable value. The detection limit (LOD) at signal/noise (S/N=3) estimated, and outstanding lower value at 94.63±4.73 pM perceived. The analytical parameters such as reproducibility, long-term performing ability and response time are found as appreciable. Finally, the projected sensor shows exceptional performances in the detection of 4-NPHyd in environmental samples.

Introduction

Generally, ZnO (zinc oxide) is a fascinating semi-conductor oxide (metal) to the material researcher for its promising physio-opto-electrochemical characteristics and terrifically it found to potentially apply in opt-electronic and electronic devices like light-emitting diodes[1], photo-detectors[2], photovoltaic cells[3], piezoelectric nano-generators [4], electroluminescence devices[5], gas sensor [6], chemical and biosensor [7,8], nano-lasers[9] and flat display devices[10] and so on. Particularly, ZnO has a wider optical band gap of 3.3 eV and 60 meV binding for exciton [11, 12], the resistivity of 1*10-3~1*105 W cm [13], stability [14] with optical transparency in the visible range. The conductivity of ZnO depends on intrinsic imperfectness like zinc interstitials and oxygen vacancies. The resistivity of ZnO for it,s wide bandgap energy can lower due to doping with the metal oxides of group III (B, Al, Ga, and In) and IV (Pb, Sn) in periodic-table [15, 16].

Several studies have shown that the nanocomposites of ZnO/SnO2 have the better physio-electro-chemical properties compared to individual metal oxide in the application as Li-ion battery [17,18], electrochemical sensors [19,20] and catalyst [21,22]. As the electrochemical sensing elements, the heterostructure of ZnO and SnO2 can enhance the inner-electric fields within the nanoparticle interfaces. As a result, the electros transfer rate between the nanoparticles increase. Due to synergistic effects the ZnO and SnO2 effects, the nanocomposites act like a buffer-matrix each to other for removing the stress and strain during electrochemical-reactions [23,24]. Thus, this approach performed to develop an electrochemical sensor by wet-chemically prepared ZnO/SnO2 NPs coated on GCE.

Due to the increasing the industrial activities, the water-soluble aromatic derivative of hydrazine coming from the untreated industrial effluent such as dyes, pesticides, photographic, plant-growth regulators, pharmaceuticals, colour and pigment industries. Besides this, the aromatic hydrazines use in explosive, rocket fuel and spacecraft fuel [25, 26]. The aromatic and aliphatic both hydrazine are poisonous for plants, animals, human and aquatic lives. Thus, hydrazine (aromatic and aliphatic) is known as carcinogenic, nephrotoxic, and environmental hazardous substance even at very lower concentration

[27,28]. The primary syndromes due to exposure of hydrazine are respiratory oedema, Sight loss for short-term, vomiting-tendency, burning in eyes and nose. The long-term exposure of hydrazine might cause a serious effect on the liver and kidney, and it also affects the central nervous system, which leads to unconsciousness [29-31]. Therefore, a reliable technique for the detection of hydrazine (4-nitrophenylhydrazine) is necessary. In recent, many kinds of research have been conducted based on CoS2–CNT nanocomposites [26], SrO.CNT NCs [27], Fe2O3 NPs [28], Co-doped ZSM-5 zeolites [25], TiO2 nanoparticles [32], Fe2O3/CeO2 nanocubes [33] and ZnO nano-urchins [29] coated on GCE for precious hydrazines detection (both aromatic and aliphatic) applying electrochemical (I-V) approach.

This experimental work performed to assemble a sensor in I-V approach selective to 4-NPHyd with ZnO/SnO2 NPs coated on GCE. A calibration plot (current versus concentration of analyte) established satisfied by linearity regression co-efficient value (R^2=99). From the slope of the calibration curve, the sensor sensitivity measured. A signal/noise (S/N) ratio of 3 used to calculate the lower detection limit (LOD). In future, applying this technique to develop the electrochemical sensor using semi-conductive binary metal oxides on GCE will be prospective in the field of environment, on a large scale.

Experimental

Materials and methods:

The analytical grade chemicals from Sigma-Andrich such as zinc acetate dihydrate, $Zn(CH_3COO)_2.2H_2O$ and tin tetrachloride ($SnCl_4$) were used to synthesize ZnO/SnO_2 NPs applying wet-chemical method in alkaline phase. The other necessary toxic chemicals known as hazardous to environment such as benzaldehyde, 4-aminophenol (4-AP), 4-nitrophenylhydrazine (4-NPHyd), 2,4-diphenyldihydrochloride (2,4-DPDHCl), 3-chlorophenol(3-CP), 3-methoxyphenol (3-MP), M-tolyl hydrazine hydrochloride (M-THydHCl), zimtaldehyde, 4-methoxyphenol (4-MP) and 3-methoxyphenylhydrazinehydrochloride (3-MPHydHCl) in analytical grade were also procured from the Sigma-Andrich USA. The auxiliary chemicals supporting to the study such mono- & disodium phosphate buffer and 5% nafion in ethanol were obtained from Sigma-Andrich also. The Thermo-Scientific XPS instrument containing A1-k-α1 radiation sources with a beam of 300.0 µm performed at 200.0 eV, and pressure 10-8 Torre was applied on the synthesized microstructures (nanomaterials) for the investigation of ionization states and binding energy of existing atoms. To confirm the structure and elemental compositions of synthesized metal oxides, the FESEM and EDS analysis were executed by an instrument model- JEOL, JSM-7600F (Japan). The grain size and crystalline plans of Ag2O-doped ZnO NSs were assessed by the implementation of powder X-ray diffraction analysis. The electrochemical characterization of ZnO/SnO_2 NPs on GCE was examined through a Keithley electrometer as the source of constant supply of potential (volts).

Preparation method of ZnO/SnO_2 NPs:

ZnO/SnO2 NPs was prepared by homogenous precipitation method using Zn(CH3COO)2. 2H2O and SnCl4 as precursors, and urea as a precipitating agent to form the alkaline phase. Following this typical

method, 5.0 mL of SnCl4 and 3.12 g (0.074 M) of Zn(CH3COO)2. 2H2O dissolved in 200 mL sized beaker and kept on a heater fixed at 90˚C with the magnetic-stirring facility. Then, 30.0 g urea was added into the mixture and continued for 4 hours at these conditions. The co-precipitate of Zn(OH)2.Sn(OH)4.nH2O obtain, and it assumed that the metal ions precipitated out totally at this high alkaline phase. Then, the resulted precipitates filtrated from the aqueous phase and successively washed with water (deionized) to remove alkalinity. Subsequently, the resultant mass placed inside an oven at 110˚C overnight to execute the complete dry. Finally, the dry metal hydroxides mixture calcined at500˚C in a muffle furnace tentatively 6 hours at a flow of atmospheric air. At this elevated temperature, the metal hydroxides oxidize into oxides form as ZnO/SnO2 nanomaterials. The obtained mixture of metal oxides then subjected to characterize by XRD, FESEM and XPS spectrometric analysis.

Modification of working electrode by ZnO/SnO_2 NPs:

The central dominating part of the electrochemical sensor is working electrode. It assembled by a GCE coated with the synthesized ZnO/SnO2 NPs. At the GCE modification process, ethanol used to form a slurry of ZnO/SnO2 NPs and deposits on the flat part of GCE to obtain a thin layer of NPs. Then, the drying of it done by keeping at the laboratory ambient conditions. For the long-time stability of deposited NPs layer on the GCE, the Nafion added. After that, the drying of modified GCE did by keeping into an oven at 35˚C for an hour. A Keithley electrometer procured from Unite States (USA) used to connect ZnO/SnO2 NPs/GCE and Pt-wire to perform as a working and counter electrodes. Then, 4-NPHyd solution at 0.1 mM diluted to several solutions varying concentrating in a range of 0.1n M~0.1 mM to electrochemical (I-V) analyze. A calibration of the 4-NPHyd sensor using current versus concentration relation executed, and linearly confirmed by regression coefficient R2. By identifying the concentration range fitted with R2=0.99, the dynamic range (LDR) for 4-NPHyd detection denoted. The sensor sensitivity calculated applying the LDR slope over the active surface area of GCE (0.0316 cm2). The signal/noise ratio (S/N=3) employed to find-out the low limit of detection (LOD) of 4-NPHyd. The mono- & disodium phosphate used as an equimolar concentration to prepare the buffer phase for electrochemical investigation. At electrochemical characterization of 4-NPHyd, the buffer phase in the investigation beaker taken 10.0 mL as constant throughout the study.

Results And Discussion

Characterizations of ZnO/SnO_2 NPs by XPS analysis:

The XPS analysis executed to evaluate the binding-energy and their oxidation number of atoms within the prepared ZnO/SnO2 NPs in Fig. 1. As the survey XPS spectrum perceived in Fig. 1(d), the obtained NPs contains only Zn2p, O1s and Sn3d orbitals. The Zn2p orbital is further sub-divided in the two asymmetric orbitals termed as Zn2p3/2 and Zn2p1/2 spin orbitals and located at 1022 and 1045 eV respectively with a separation of 23 eV, confirmed the Zn2+ ionization state in the NPs of ZnO/SnO2 NPs demonstrated in Fig.1 (a) [34-37].

The XPS spectral peak showing the high intensity located at 530.8 eV in Fig. 1(b) is identified of O1s and identified to lattice oxygen of ionization state of O2- in the prepared ZnO/SnO2 NPs [38-40]. Besides this, the Sn3d level orbital in Fig. 1(c) is sub-divided in the two spin orbitals shown the binding energies of 486.5 and 495.25 eV related to Sn3d5/2 and Sn3d3/2 orbitals respectively. These spin orbitals separate with 8.7 eV a typical value confirms the Sn4+oxidation identified by the earlier articles [41,42].

The morphology of elemental compositions analysis of ZnO/SnO_2 NPs:

The structural and atomic compositions of ZnO/SnO2 nanomaterials identified by FESEM and EDS analysis.

A pictorial in Fig. 2(a) and Fig.2 (b), the magnifying (low and high) images of prepared nanomaterials, the ZnO, and SnO2 nanomaterials are aggregated irregularly to form the nanoparticle shape with distinct sizes and shapes. The EDS image shown in Fig. 2(c) is conformed the same observation as in Fig. 1(a,b). The EDS elemental analysis illustrated in Fig. 2(d), the synthesized NPs contains 28.61% O, 33.7% Zn and 37.69% Sn only and the peaks associated with impurities are not detected.

The evaluation of phase crystallinity and particles size by XRD pattern:

The XRD pattern of ZnO/SnO2 NPs shows in Fig. 3, and X-ray powder diffraction (XRD) taken to identify the crystalline phases of ZnO-SnO2 at the range of 20–80◦ with Cu Kα1 radiation (λ =1.5406 A°). The reflected peaks regarding ZnO such as (002), (101), (110), (201), (004) and (202) plans can index following JCPDS (Joint Committee on Powder Diffraction Standards) card no 0089-1397 and previously reported articles of ZnO nanoparticles [43,44]. Besides this, the identified peaks for SnO2 such as (110), (211), (220), (311) and (301) plans are conformed by JCPDD No. 0036-1451 and previous authors [45, 46]. The average crystal size of synthesized NPs calculates applying the Scherer formula as D= (0.94λ)/(βCosθ), and the estimated crystal size using ZnO(002) is 10.85 nm.

Sensor application of ZnO/SnO_2 NPs/GCE Assembly:

The selective 4-NPHyd sensor assembled by the coating of a GCE with ZnO/SnO2 NPs as a layer of NPs and applied to the detection of 4-NPHyd at a buffer of pH 7.0. The long-time stability of NPs layer on GCE boosted by the addition of Nafion suspension. It should know that the Nafion used as a binder is a copolymer with conductive in nature. Thus, the use of Nafion on the modified GCE improves the conductance and the electron transfer rate of the resultant sensor. The similar characteristic of the sensor assembled using Nafion has reported in several articles to detect toxic chemicals [47-51]. The wet-chemically prepared ZnO/SnO2 NPs on GCE as an electrochemical sensor to selective detection of 4-NPHyd is new and the information regarding its not available. During the electrochemical (I-V) sensing of 4-NPHyd in the buffer solution, the holding time in Keithley electrometer set 1.0 s as constant throughout the study. The amount of buffer solution for each I-V investigation took 10 mL in the measuring beaker.

The toxic chemicals in analytical grade such as benzaldehyde, 4-AP, 4-NPHyd, 2,4-DPDHCl, 3-CP, 3-MP, M-THydHCl, zimtaldehyde, 4-MP and 3-MPHydHCl were subjected to I-V investigation by assembled sensor based on ZnO/SnO2 NPs/GCE at first illustrated in Fig. 3(a). The 4-NPHyd shows the supreme I-V outcome among the investigating toxics chemicals, which performed at 0.1μM and 0~+1.5 V in 7.0 pH buffer phase presented in Fig. 4(a). Therefore, considering the highest I-V outcome, 4-NPHyd is categorised to selective toxic for the sensor assembly. Then, 4-NPHyd solutions in a range of 0.1nM~ 0.1 mM applied to analysis electrochemically at 0~+1.5 V potential range in a buffer solution, and the resulted data represents in Fig. 4(b). The illustrated data in Fig. 4(b) exhibits a pattern to increase the I-V intensity with the increasing concentration of 4-NPHyd from lower to higher. This patter has described by previous authors in the detection of toxic chemicals in earlier [52-57]. The calibration of the 4-NPHyd sensor plotted in Fig. 4(c) known as a calibration curve. To execute this calibration, the current data separated from Fig. 4(b) at +1.5 volt. From the observation of Fig. 4(c), the current data are distributed linearly on the calibration curve from 0.1nM to 0.01 mM of 4-NPHyd defined as the dynamic range of detection (LDR) and the linearity is satisfied by the regression co-efficient R2=0.9976. The defined LDR has quite a wide range of detection of 4-NPHyd.

The sensor sensitivity using the calibration curve slope and active surface area of GCE (0.0316 cm2) is calculated and an appreciable sensitivity at 7.6930 μAμM-1cm-2 perceive. The detection limit (LOD)of the 4-NPHyd sensor estimates by considering the signal/noise (S/N=3) and the satisfactory LOD around 94.63±4.73 pM achieve.

The sensor response time expresses as a time to require the completion of an I-V analysis of an analyte, and it is an efficiency measuring parameter. The response time of 4-NPHyd sensor tested at 0.1μM of 4-NPHyd in the buffer phase of pH 7.0 shown in Fig. 5(a). As perceived in Fig. 5(a), the current responses become steady around 22.0 s. Thus, the 4-NPHyd sensor needs 22.0 s to complete the I-V analysis of 4-NPHyd in the buffer phase. 22.0 s is quite enough to prove the high efficiency of the 4-NPHyd sensor with ZnO/SnO2 NPs/GCE. The GCE was modified with SnO2 NPs and ZnO/SnO2 NPs to execute control experiments at 0.1μ 4-NPHyd and 0~+1.5 V in a buffer solution as illustrated in Fig. 5(b). As in Fig. 5(b), ZnO/SnO2 NPs/GCE electrode is exhibited the higher electrochemical activity compared to single SnO2 NPs. It happens due to the combinational effects of both metal oxides. The reproducibility is reliability measuring parameter of the sensor and defines as the capability of the sensor to generate the unique I-V outcome in the identical conditions. The reproducibility test at 0.1μM of 4-NPHyd and 0~+1.5V in buffer phase of pH 7.0 was performed demonstrated in Fig. 5(c) in successive seven hours in a day. As shown in Fig. 5(c), the seven tests are unique and impossible to distinguish each to other. Thus, the 4-NPHyd sensor shows notable information that it is well enough to detect 4-NPHyd in unknown samples reliably. To measure the precision of reproducibility parameter in term of %RSD (relative standard deviation), the current data at +1.5 V were subjected to check its precision and found 1.39% RSD, provides the high precision of reproducibility parameter. The stability of the sensor in the buffer phase is a very important criterion. To check this parameter of the 4-NPHyd sensor, the similar reproducibility tests but in successive seven days were executed illustrated in Fig. 5(d). The results alike reproducibility are

perceived. This test conforms to the long-term stability of the sensor in the buffer phase with consistency in performance.

During the electrochemical detection of 4-nitrophenylhydrazine in buffer phase at applied potential, the 4-nitrophenylhydrazine molecules are adsorbed on the layered surface of ZnO/SnO_2 NPs and influence of potential, it is oxidized to 1,4-diaminobenzene and ammonium ion. Sometime, a number of free electrons are generated, which are responsible to enhance the conductance of sensing buffer medium and finally, I-V response is recorded in Keithely electrometer. Similar electrochemical oxidation has been mentioned in the earlier reports [58-60].

To execute the validation of this study, the researches of similar are compared with this study in-term of parameters such as sensitivity, LDR and detection limit (DL) as illustrated in Table 1[61-63] and considering the parameters, the performances of this study is found as quite satisfactory and appreciable.

Table 1: The comparison of analytical performances of 4-NPHyd sensors based on ZnO/SnO_2 NPs/GCE.

Modified GCE	Analyte	*DL	#LDR	Sensitivity	Ref.
CoS_2/CNT NCs/GCE	*Hyd*	*0.1 nM*	*0.1 nM~1.0 mM*	*0.0044 $\mu A \mu M^{-1} m^{-2}$*	*[61]*
Sn/ZnO NPs/GCE	*Hyd*	*18.9 pM*	*2.0 nM ~20.0 mM*	*5.0108 $\mu A \mu M^{-1} m^{-2}$*	*[62]*
T-PANI/Ag NCs/GCE	*Hyd*	*2.8 nM*	*0.01μ–10 mM*	*12.5 $\mu A \mu M^{-1} m^{-2}$*	*[63]*
ZnO/SnO_2 NPs/GCE	*4-NPHyd*	*94.6 pM*	*0.1nM ~0.01mM*	*7.6930 $\mu A \mu M^{-1} m^{-2}$*	*This work*

**DL (detection limit), #LDR (linear dynamic range), pM(picomole), mM(millimole).*

Analysis of real environmental samples:

The validation of the proposed 4-NPHyd sensor based on ZnO/SnO_2 NPs/GCE in detecting 4-NPHyd was performed by applying recovery method. For this experiment, the samples known as real environmental samples collected as the extract of PC-water bottle, food packaging bag and sea and tape water. The analyzed data are presented in Table 2 and found as satisfactory.

Table 2. The analysis of real environmental samples using ZnO/SnO_2 NPs/GCE chemical sensor by recovery method.

Sample	Added 4-NPHyd concentration (μM)	Measured 4-NPHyd conc.[a] by ZnO/SnO_2 NPs/GCE(μM)			Average recovery[b] (%)	RSD[c] (%) (n=3)
		R1	R2	R3		
Sea water	*0.0100*	*0.0104*	*0.0104*	*0.0106*	*104.54*	*1.10*
PC- water bottle	*0.0100*	*0.0096*	*0.0094*	*0.0094*	*95.17*	*1.22*
PVC- food packaging bag	*0.0100*	*0.0105*	*0.0106*	*0.0109*	*106.89*	*1.95*
Tape water	*0.0100*	*0.0104*	*0.0103*	*0.0103*	*103.08*	*0.56*

[a]*Mean of three repeated determination (signal to noise ratio 3) ZnO/SnO_2 NPs/GCE*

[b]*Concentration of 4-NPHyd determined/Concentration taken. (Unit:nM)*

[c]*Relative standard deviation value indicates precision among three repeated measurements(R1,R2,R3).*

Conclusion

The wet-chemical prepared ZnO/SnO_2 NPs in alkaline phase were characterized by XPS, FESEM, EDS and X-ray diffraction at ambient condition. The prepared NPs were deposited on GCE to result 4-NPHyd sensor in buffer phase. A plot executed from concentration of 4-NPHyd versus current known as calibration curve and used to calculate sensor sensitivity, LDR and DL found as appreciable. The 4-NPHyd sensor parameters such as reproducibility, response time and long-time performing ability were tested and outstanding outcomes were exhibited.

Declarations

Conflicts of interest statement:

The authors declare that they have no known competing financial interests or personal relationships that could have appeared to influence the work reported in this paper.

Acknowledgements:

Center of Excellence for Advanced Materials Research (CEAMR), Chemistry Department, King Abdulaziz University, Jeddah, Saudi Arabia is highly acknowledged for financial supports and research facilities.

References

1. J.H. Na, M. Kitamura, M. Arita, Y. Arakawa. Hybrid junction light-emitting diodes based on sputtered ZnO and organic semiconductors. Appl. Phys. Lett. 95 (2009) 253303-253305.

2. C.Y. Lu, S.J. Chang, S.P. Chang, C.T. Lee, C.F. Kuo, H.M. Chang, H.Z. Chiou, C.L. Hsu, I.C. Chen. Ultraviolet photodetectors with ZnO nanowires prepared on ZnO: Ga/glass templates, Appl. Phys. Lett. 89 (2006) 153101-153103.
3. P. Sudhagar, R.S. Kumar, J.H. Jung, W. Cho, R. Sathyamoorthy, J. Won,Y.S. Kang. Facile synthesis of highly branched jacks-like ZnO nanorods and their applications in dye-sensitized solar cells. Mater. Res. Bull. 46 (2011) 1473-1479.
4. Z.L. Wang, R. Yang, J. Zhou, Y. Qin, C. Xu, Y. Hu, S. Xu. Lateral nanowire/nanobelt based nanogenerators, piezotronics and piezo-phototronics. Mater. Sci. Eng., R 70 (2010) 320-329.
5. W.I. Park, G.C. Yi. Electroluminescence in n-ZnO nanorod arrays vertically grown on p-GaN. Adv. Mater. 16 (2004) 87-90.
6. J. Xu, J. Han, Y. Zhang, Ya. Sun, B. Xie. Studies on alcohol sensing mechanism of ZnO based gas sensors. Sens. Actuators, B: Chem. 132 (2008) 334-339.
7. M.T. Uddin, M.M. Alam, A.M. Asiri, M.M. Rahman, T. Toupance, M.A. Islam. Electrochemical detection of 2-nitrophenol using a heterostructure ZnO/RuO_2 nanoparticle modified glassy carbon electrode. RSC Adv. 10 (2020) 122–132.
8. M.M. Alam, A.M. Asiri, M.T. Uddin, M.A. Islam, M.R. Awual, M.M. Rahman. Detection of uric acid based on doped ZnO/Ag_2O/Co_3O_4 nanoparticle loaded glassy carbon electrode. New J. Chem. 43 (2019) 8651-8659.
9. M.H. Huang, S. Mao, H. Feick, H. Yan, Y. Wu, H. Kind, E. Webber, R. Russo, P. Yang. Room-temperature ultraviolet nanowire nanolasers. Science. 292 (2001) 1897-1899.
10. S.B. Park, B.G. Kim, J.Y. Kim, T.H. Jung, D.G. Lim, J.H. Park, J.G. Park. Field-emission properties of patterned ZnO nanowires on 2.5 D MEMS substrate. Appl. Phys. A 102 (2011) 169-172.
11. A.k. Ramadoss, S.J. Kim. Facile preparation and electrochemical characterization of graphene/ZnO nanocomposite for supercapacitor applications. Materials Chemistry and Physics. 140 (2013) 405-411.
12. H. Benzarouk, A. Drici, M. Mekhnache, A. Amara, M. Guerioune, J.C. Bernède, H. Bendjffal. Effect of different dopant elements (Al, Mg and Ni) on microstructural, optical and electrochemical properties of ZnO thin films deposited by spray pyrolysis (SP). Superlattices and Microstructures. 52 (2012) 594–604.
13. H. Ki Kim, K. Sung Lee, H. Ah Kang. Characteristics of indium zinc oxide top cathode layers grown by box cathode sputtering for top-emitting organic light-emitting diodes. Journal of Electrochemical Society. 153 (2006) H29–H33.
14. G. Fang, D. Li, Bao-Lun Yao. Fabrication and characterization of transparent conductive ZnO:Al thin films prepared by direct current magnetron sputtering with highly conductive ZnO($ZnAl_2O_4$) ceramic target. Journal of Crystal Growth. 247 (2003) 393–400.
15. A. Bougrine, A. El Hichou, M. Addou, J. Ebothé, A. Kachouane, M. Troyon. Structural, optical and cathodoluminescence characteristics of undoped and tin-doped ZnO thin films prepared by spray

pyrolysis. Materials Chemistry and Physics. 80 (2003) 438–445.

16. J. Bian, X. Li, L. Chen, Q. Yao. Properties of undoped n-type ZnO film and N–In codoped p-type ZnO film deposited by ultrasonic spray pyrolysis. Chemical Physics Letters. 393 (2004) 256–259.
17. F. Belliard, J.T.S. Irvine. Electrochemical performance of ball-milled ZnO–SnO_2 systems as anodes in lithium-ion battery. J. Power Sources. 97–98 (2001) 219–222.
18. M. Ahmad, S. Yingying, H.Y. Sun, W.C. Shen, J. Zhu. SnO_2/ZnO composite structure for the lithium-ion battery electrode. J. Solid State Chem. 196 (2012) 326–331.
19. S.H. Yan, S.Y. Ma, X.L. Xu, W.Q. Li, J. Luo, W.X. Jin, T.T. Wang, X.H. Jiang, Y. Lu, H. S. Song. Preparation of SnO_2–ZnO hetero-nanofibers and their application in acetone sensing performance. Mater. Lett. 159 (2015) 447–450.
20. S.H. Yan, S.Y. Ma, W.Q. Li, X.L. Xu, L. Cheng, H.S. Song, X.Y. Liang. Synthesis of SnO_2–ZnO heterostructured nanofibers for enhanced ethanol gas-sensing performance. Sens. Actuators B: Chem. 221 (2015) 88–95.
21. J.J. Kong, Z.B. Rui, H.B. Ji, Y.X. Tong. Facile synthesis of ZnO/SnO_2 hetero nanotubes with enhanced electrocatalytic property. Catal. Today. 258 (2015) 75–82.
22. R. Lamba, A. Umar, S.K. Mehta, S.K. Kansal. ZnO doped SnO_2 nanoparticles heterojunction photo-catalyst for environmental remediation. J. Alloy. Compd. 653 (2015) 327–333.
23. N. Feng, L. Qiao, D.K. Hu, X.L. Sun, P. Wang, D.Y. He. Synthesis, characterization, and lithium-storage of ZnO–SnO_2 hierarchical architectures. RSC Adv. 3 (2013) 7758–7764.
24. L. Luo, W. Xu, Z. Xia, Y. Fei, J. Zhu, C. Chen, Y. Lu, Q. Wei, H. Qiao, X. Zhang. Electrospun ZnO–SnO_2 composite nanofibers with enhanced electrochemical performance as lithium-ion anodes. Ceramics International. 42 (2016) 10826–10832.
25. M.M. Rahman, B.M. Abu-Zied, A.M. Asiri. Ultrasensitive hydrazine sensor fabrication based on Co-doped ZSM-5 zeolites for environmental safety. RSC Adv. 7 (2017) 21164–21174.
26. M.M. Rahman, J. Ahmed, A.M. Asiri, I.A. Siddiquey, M.A. Hasnat. Development of highly-sensitive hydrazine sensor based on facile CoS_2-CNT nanocomposites. RSC Adv. 6 (2016) 90470–90479.
27. M.M. Rahman, M.M. Hussain, A.M. Asiri. A novel approach towards hydrazine sensor development using SrO●CNT nanocomposites. RSC Adv. 6 (2016) 65338–65348.
28. H. Akhter, J. Murshed, M.A. Rashed, Y. Oshim, Y. Nagao, M.M. Rahman, A.M. Asiri, M.A. Hasnat, M.N. Uddin, I.A. Siddiquey. Fabrication of hydrazine sensor based on silica-coated Fe_2O_3 magnetic nanoparticles prepared by a rapid microwave irradiation method. Journal of Alloys and Compounds. 698 (2017) 921-929.
29. A. Umar, M.S. Akhtar, A. Al-Hajry, M.S. Al-Assiri, G.N. Dar, M.S. Islam. Enhanced photocatalytic degradation of harmful dye and phenyl hydrazine chemical sensing using ZnO nanourchins. Chemical Engineering Journal. 262 (2015) 588–596.
30. M.M. Rahman, S.B. Khan, A. Jamal, M. Faisal, A.M. Asiri. Fabrication of Phenyl-Hydrazine Chemical Sensor Based on Al- doped ZnO Nanoparticles. Sensors & Transducers Journal. 134 (2011) 32-44.

31. H.M. Nassef, A.E. Radi, C.K. O'Sullivan. Electrocatalytic oxidation of hydrazine at o-aminophenol grafted modified glassy carbon electrode: Reusable hydrazine amperometric sensor. Journal of Electroanalytical Chemistry. 592 (2006) 139–146.
32. M.M. Rahman, V.G. Alfonso, F. Fabregat-Santiago, J. Bisquert, A.M. Asiri, A.A. Alshehri, H.A. Albar. Hydrazine sensors development based on a glassy carbon electrode modified with a nanostructured TiO_2 films by electrochemical approach. Microchim. Acta. 184 (2017) 2123–2129.
33. M.M. Rahman, M.M. Alam, A.M. Asiri. Selective hydrazine sensor fabrication with facile low-dimensional Fe_2O_3/CeO_2 nanocubes. New J. Chem. 42 (2018) 10263-10270.
34. M.M. Rahman, M.M. Alam, A.M. Asiri, M.A. Islam. Ethanol sensor development based on ternary-doped metal oxides ($CdO/ZnO/Yb_2O_3$) nanosheets for environmental safety. RSC Adv. 7 (2017) 22627–22639.
35. M.M. Rahman, M.M. Alam, A.M. Asiri, M.R. Awual. Fabrication of 4-aminophenol sensor based on hydrothermally prepared ZnO/Yb_2O_3 nanosheets. New J. Chem. 41 (2017) 9159—9169.
36. M.M. Alam, A.M. Asiri, M.T. Uddin, M.A. Islam, M.M. Rahman. Wet-chemically prepared low-dimensional $ZnO/Al_2O_3/Cr_2O_3$ nanoparticles for xanthine sensor development using an electrochemical method. RSC Adv. 8 (2018) 12562–12572.
37. M.M. Rahman, M.M. Alam, A.M. Asiri. Carbon black co-adsorbed ZnO nanocomposites for selective benzaldehyde sensor development by electrochemical approach for environmental safety. Journal of Industrial and Engineering Chemistry. 65 (2018) 300–308.
38. M.M. Alam, A.M. Asiri, M.T. Uddin, M.A. Islam, M.M. Rahman. In-situ Glycine Sensor Development Based $ZnO/Al_2O_3/Cr_2O_3$ Nanoparticles. ChemistrySelect. 3 (2018) 11460–11468.
39. M.M. Alam, A.M. Asiri, M.T. Uddin, Inamuddin, M.A. Islam, M.R. Awual, M.M. Rahman. One-step wet-chemical synthesis of ternary $ZnO/CuO/Co_3O_4$ nanoparticles for sensitive and selective melamine sensor development. New J. Chem. 43 (2019) 4849-4858.
40. M.A. Subhan, S.S. Jhuma, P.C. Saha, M.M. Alam, A.M. Asiri, M. Al-Mamun, S.A. Attia, T.H. Emon, A.K. Azad, M.M. Rahman. Efficient selective 4-aminophenol sensing and antibacterial activity of ternary $Ag_2O_3.SnO_2.Cr_2O_3$ nanoparticles. New J. Chem. 43 (2019) 10352-10365.
41. M.M. Rahman, M.M. Alam, A.M. Asiri. Fabrication of an acetone sensor based on facile ternary $MnO_2/Gd_2O_3/SnO_2$ nanosheets for environmental safety. New J. Chem. 41 (2017) 9938-9946.
42. M.M. Rahman, M.M. Alam, A.M. Asiri, M.A. Islam. Fabrication of selective chemical sensor with ternary $ZnO/SnO_2/Yb_2O_3$ nanoparticles. Talanta. 170 (2017) 215–223.
43. M. Saliani, R. Jalal, E.K. Goharshadi, Effects of pH and Temperature on Antibacterial Activity of Zinc Oxide Nanofluid Against Escherichia coli O157: H7 and Staphylococcus aureus. Jundishapur J. Microbiol. 8 (2015) 17115.
44. S. Sagadevan, J. Podder. Investigation on Structural, Surface Morphological and Dielectric Properties of Zn-doped SnO_2 Nanoparticles. Materials Research. 19 (2016) 420-425.

45. W. Chen, Q. Zhou, F. Wan, T. Gao. Gas Sensing Properties andMechanism of Nano-SnO2-Based Sensor for Hydrogen and Carbon Monoxide. Journal of Nanomaterials. (2012) 612420.
46. E. Janardhan, M.M. Reddy, P.V. Reddy, M.J. Reddy. Synthesis of SnO Nanopatricles—A Hydrothermal Approach. World Journal of Nano Science and Engineering. 8 (2018) 33-37.
47. M.M. Rahman, M.M. Alam, A.M. Asiri. Potential application of mixed metal oxide nanoparticle-embedded glassy carbon electrode as a selective 1,4-dioxane chemical sensor probe by an electrochemical approach. RSC Adv. 9 (2019) 42050–42061.
48. R.H. Rakib, M.A. Hasnat, M.N. Uddin, M.M. Alam, A.M. Asiri, M.M. Rahman, I.A. Siddiquey. Fabrication of a 3,4-Diaminotoluene Sensor Based on a TiO_2-Al_2O_3 Nanocomposite Synthesized by a Fast and Facile Microwave Irradiation Method. ChemistrySelect. 4 (2019) 12592–12600.
49. M.M. Rahman, M.M. Alam, A.M. Asiri. Detection of toxic choline based on Mn_2O_3/NiO nanomaterials by an electrochemical method. RSC Adv. 9 (2019) 35146–35157.
50. M.M. Rahman, M.M. Alam, K.A. Alamry. Sensitive and selective m-tolyl hydrazine chemical sensor development based on CdO nanomaterial decorated multi-walled carbon nanotubes. Journal of Industrial and Engineering Chemistry. 77 (2019) 309–316.
51. B.M. Abu-Zied, M.M. Alam, A.M. Asiri, W. Schwieger, M.M. Rahman. Fabrication of 1,2-dichlorobenzene sensor based on mesoporous MCM-41material. Colloids and Surfaces A. 562 (2019) 161–169.
52. M.M. Rahman, M.M. Alam, A.M. Asiri. Development of an efficient phenolic sensor based on facile Ag_2O/Sb_2O_3 nanoparticles for environmental safety. Nanoscale Adv. 1 (2019) 696–705.
53. M.R. Karim, M.M. Alam, M.O. Aijaz, A.M. Asiri, M.A. Dar, M.M. Rahman. Fabrication of 1,4-dioxane sensor based on microwave assisted PAni-SiO_2 nanocomposites. Talanta 193 (2019) 64–69.
54. M.M. Rahman, A. Wahid, M.M. Alam, A.M. Asiri. Efficient 4-Nitrophenol sensor development based on facile Ag@Nd_2O_3 nanoparticles. Materials Today Communications 16 (2018) 307–313.
55. M.M. Rahman, M.M. Alam, A.M. Asiri. Selective hydrazine sensor fabrication with facile low-dimensional Fe_2O_3/CeO_2 nanocubes. New J. Chem. 42 (2018) 10263-10270.
56. M.M. Rahman, M.M. Alam, A.M. Asiri, M.A. Islam. 3,4-Diaminotoluene sensor development based on hydrothermally prepared $MnCo_xO_y$ nanoparticles. Talanta 176 (2018) 17–25.
57. M.M. Rahman, M.M. Alam, A.M. Asiri. Sensitive 1,2-dichlorobenzene chemi-sensor development based on solvothermally prepared FeO/CdO nanocubes for environmental safety. Journal of Industrial and Engineering Chemistry 62 (2018) 392–400.
58. S. Sundaram, A.S. Kumar, M. Jagannathan, M.R.A. Kadir. In situ stabilization of hydroxylamine via electrochemical immobilization of 4-nitrophenol on GCE/MWCNT electrodes: NADH electrocatalysis at zero potential. Anal. Methods 6 (2014) 8894-8900.
59. B. Kaur, R. Srivastava, B. Satpati. Copper nanoparticles decorated polyaniline–zeolite nanocomposite for the nanomolar simultaneous detection of hydrazine and phenylhydrazine. Catal. Sci. Technol. 6 (2016) 1134-1145.

60. M.M. Hussain, M.M. Rahman, A.M. Asiri. Efficient 2-Nitrophenol Chemical Sensor Development Based on Ce2O3 Nanoparticles Decorated CNT Nanocomposites for Environmental Safety. PLOS ONE (2016).
61. M.M. Rahman, J. Ahmed, A.M. Asiri, I.A. Siddiquey, M.A. Hasnat. Development of highly-sensitive hydrazine sensor based on facile CoS_2–CNT nanocomposites. RSC Adv. 6 (2016) 90470–90479.
62. M.M. Rahman, H.B. Balkhoyor, A.M. Asiri. Ultrasensitive and selective hydrazine sensor development based on Sn/ZnO nanoparticles. RSC Adv. 6 (2016) 29342-29352.
63. M.M. Rahman, A. Khan, H.M. Marwani, A.M. Asiri. Hydrazine sensor based on silver nanoparticle-decorated polyaniline tungstophosphate nanocomposite for use in environmental remediation. Microchim Acta. 183 (2016) 1787–1796.

Figures

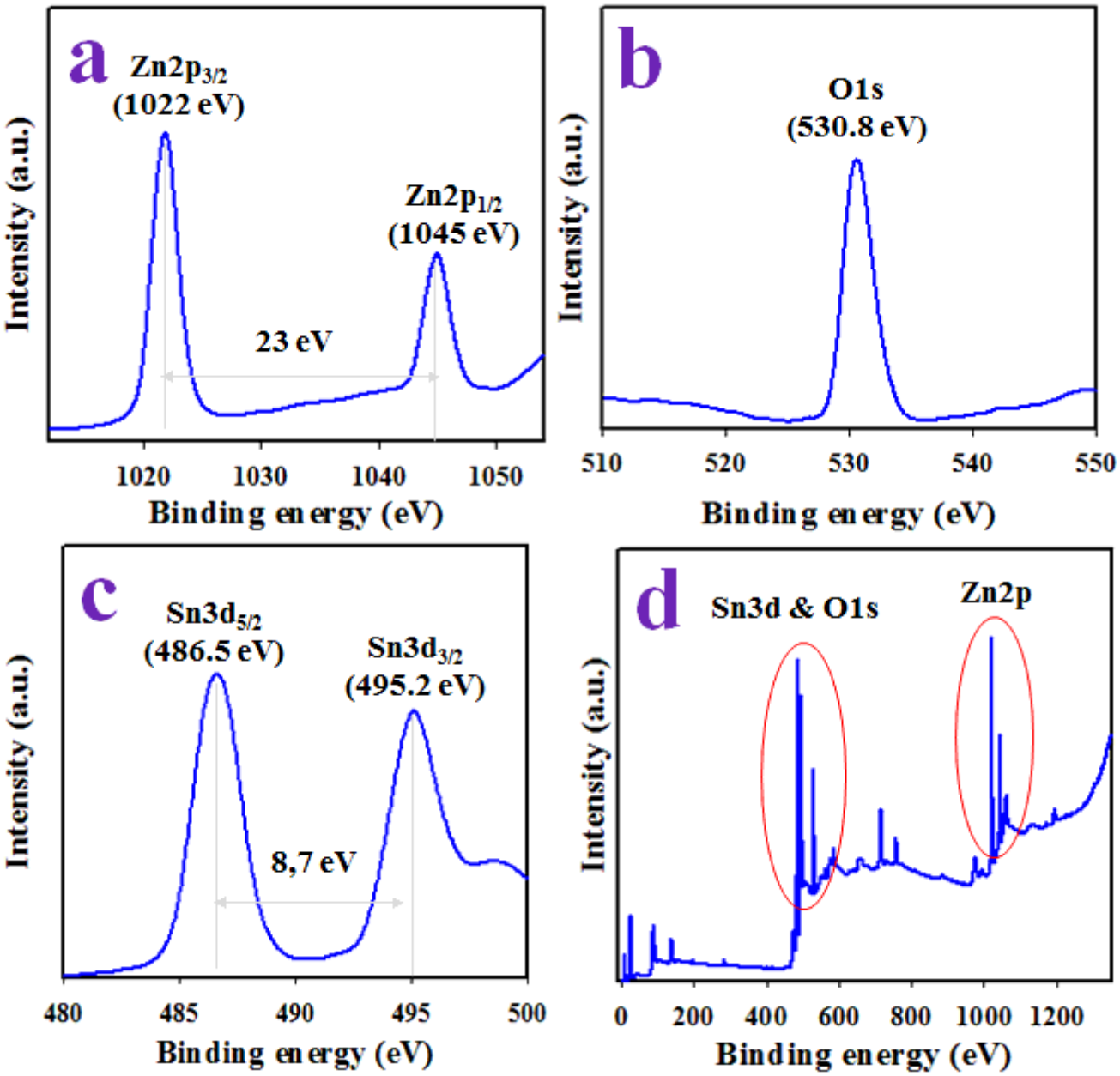

Figure 1

The XPS spectra of wet-chemically synthesized ZnO/SnO2 NPs in alkaline phase. (a) The asymmetric spin orbitals of Zn2p level, (b) O1s peak, (c) the core level Sn3d orbited splitting into two spin orbitals of Sn3d5/2 and Sn3d3/2 and (d) the survey XPS spectra of ZnO/SnO2 NPs.

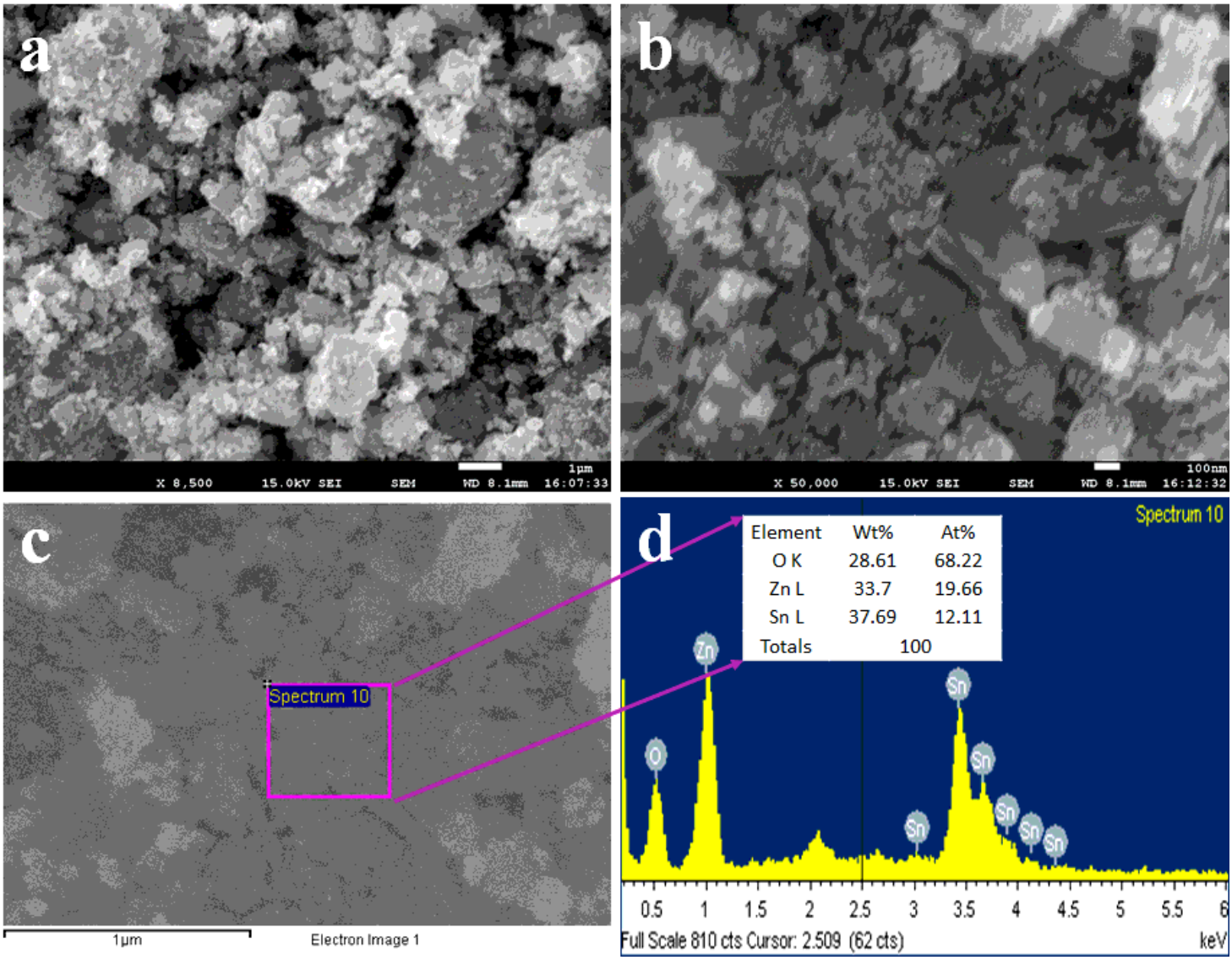

Figure 2

(a,b) The low and high magnifying images of ZnO/SnO2 NPs and (c,d) the EDS image and elemental analysis of NPs.

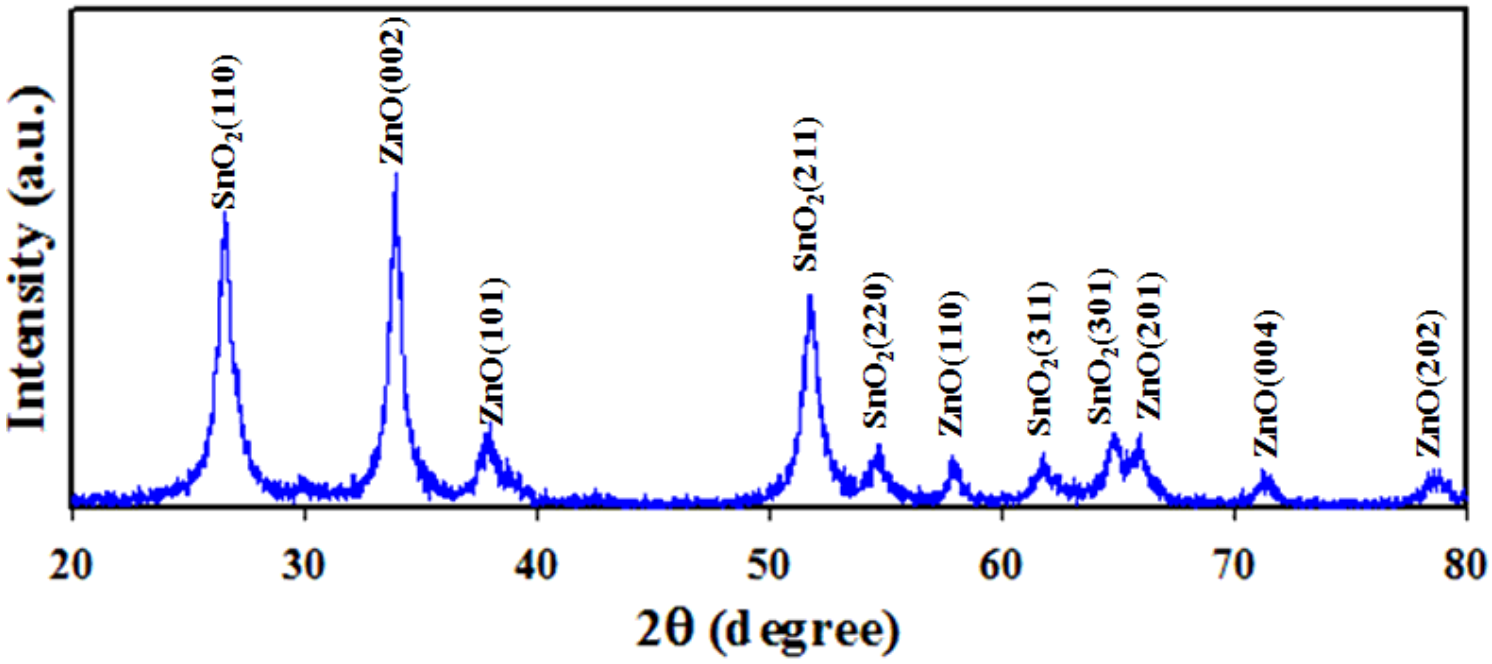

Figure 3

The XRD pattern of wet-chemically prepared ZnO/SnO2 NPs.

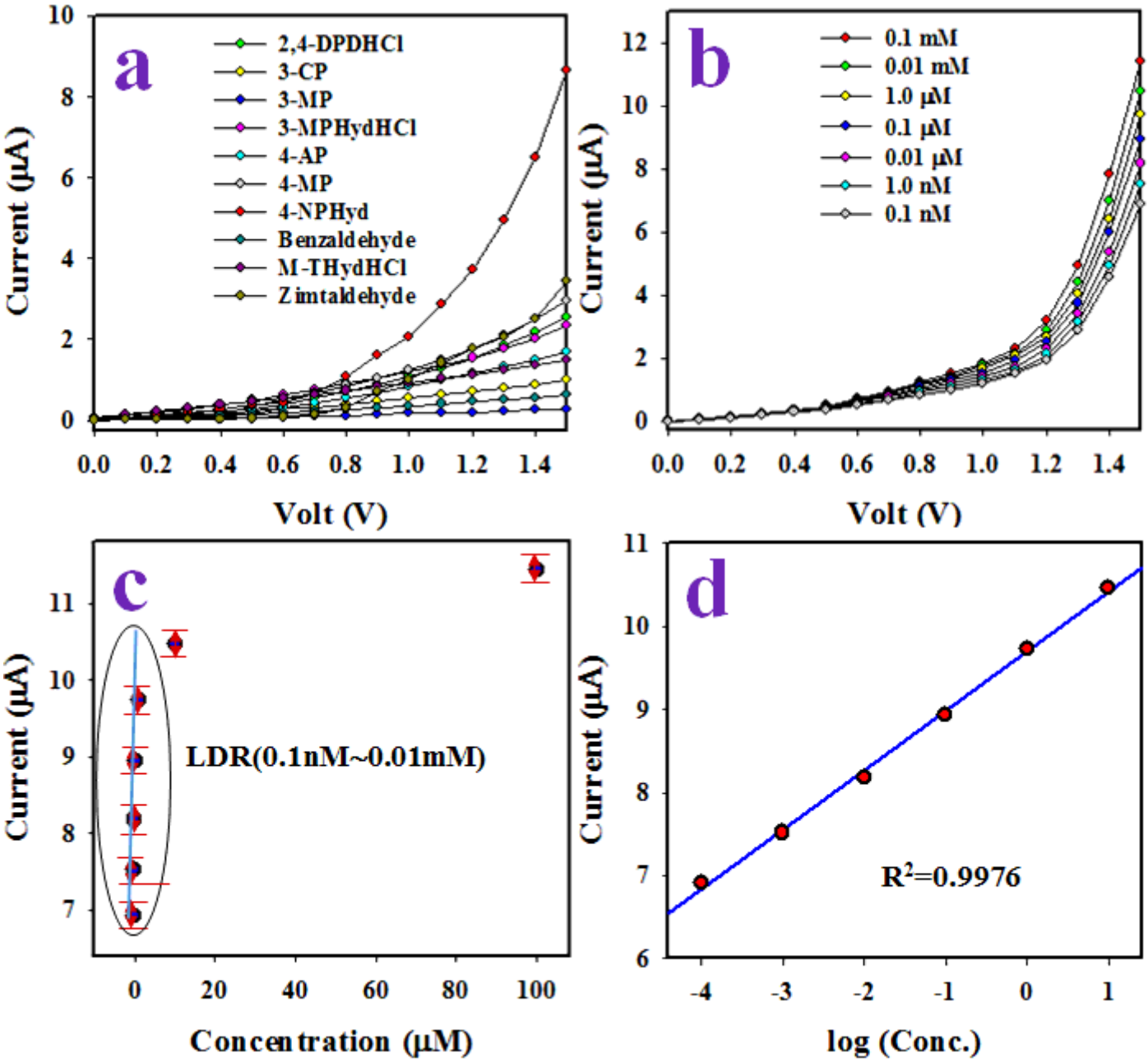

Figure 4

The electrochemical characterization of assembled sensor with ZnO/SnO2 NPs/GCE. (a) the investigation of electrochemical responses of toxics chemical of 0.1µM in buffer phase, (b) I-V outcome of 4-NPHyd based on concentration, (c) the calibration of 4-NPHyd sensor and (d) current versus conc. [inset current versus log(conc.)]

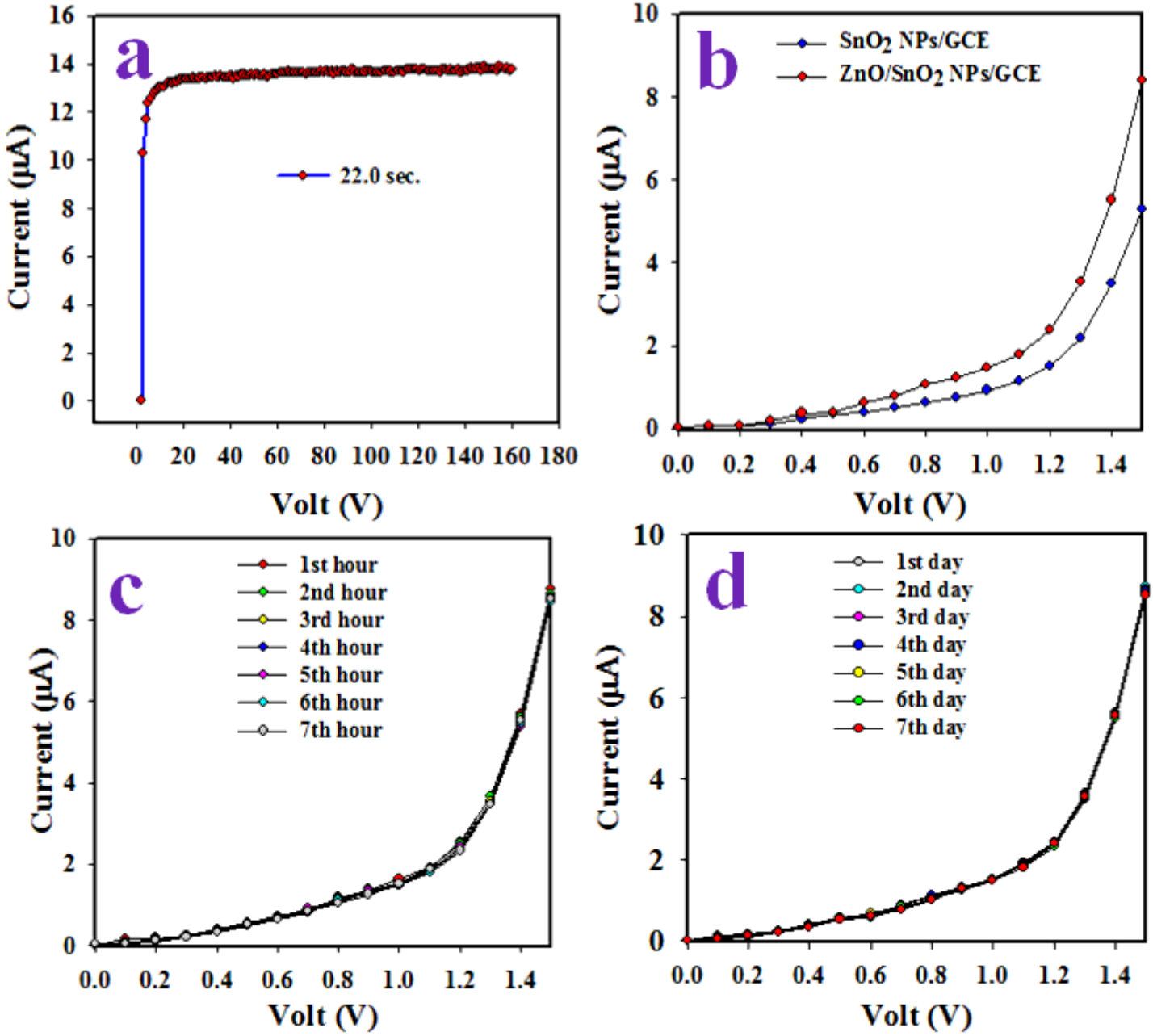

Figure 5

The tests of 4-NPHyd sensor based on ZnO/SnO2 NPs/GCE to execute its reliability. (a) Response time, (b) the control experiments for 4-NPHyd sensor at 0.1μ 4-NPHyd and 0~+1.5 V in buffer solution, (c) reproducibility test at 0.1μ 4-NPHyd and 0~+1.5 V in buffer solution and (d) stability of 4-NPHyd sensor.

Supplementary Files

This is a list of supplementary files associated with this preprint. Click to download.

- Onlinefloatimage6.png